

The following resources related to this article are available online at www.sciencemag.org (this information is current as of November 12, 2009):

Updated information and services, including high-resolution figures, can be found in the online version of this article at:

<http://www.sciencemag.org/cgi/content/full/317/5839/803>

Supporting Online Material can be found at:

<http://www.sciencemag.org/cgi/content/full/317/5839/803/DC1>

A list of selected additional articles on the Science Web sites **related to this article** can be found at:

<http://www.sciencemag.org/cgi/content/full/317/5839/803#related-content>

This article **cites 22 articles**, 10 of which can be accessed for free:

<http://www.sciencemag.org/cgi/content/full/317/5839/803#otherarticles>

This article has been **cited by** 50 article(s) on the ISI Web of Science.

This article has been **cited by** 19 articles hosted by HighWire Press; see:

<http://www.sciencemag.org/cgi/content/full/317/5839/803#otherarticles>

This article appears in the following **subject collections**:

Cell Biology

http://www.sciencemag.org/cgi/collection/cell_biol

Information about obtaining **reprints** of this article or about obtaining **permission to reproduce this article** in whole or in part can be found at:

<http://www.sciencemag.org/about/permissions.dtl>

assistance, and reagents; F. Sacerdoti for invaluable help with computational resources; and A. Weber for editorial assistance. This research was supported in part by a grant from the Israel Science Foundation to I.T.A. A version of Desmond, the software used to perform the simulations described in this article, will be released by the end of 2007. This version will be made available by D. E. Shaw Research for noncommercial research use and by Schrödinger LLC for commercial use. Before release, the current version of Desmond will be available from the authors upon request under conditions described in the

SOM. D. E. Shaw Research and Schrödinger have entered into a licensing agreement for the commercial distribution of Desmond by Schrödinger. D.E.S. has a beneficial ownership interest in D. E. Shaw Research, and R.O.D., M.P.E., J.L.K., I.K., Y.S., and D.E.S. have beneficial ownership interests in Schrödinger. Each of these authors may thus benefit financially from any resulting sales of Desmond. D.E.S. is a member of the Board of Directors of the American Association for the Advancement of Science (AAAS), the publisher of *Science*, and serves as treasurer of the AAAS.

Supporting Online Material

www.sciencemag.org/cgi/content/full/317/5839/799/DC1
Materials and Methods
SOM Text
Figs. S1 to S4
Tables S1 to S4
References
Detailed Statement of Software Availability

21 March 2007; accepted 28 June 2007
10.1126/science.1142824

Augmented Wnt Signaling in a Mammalian Model of Accelerated Aging

Hongjun Liu,¹ Maria M Fergusson,^{1*} Rogerio M. Castilho,^{2*} Jie Liu,¹ Liu Cao,¹ Jichun Chen,³ Daniela Malide,⁴ Ilsa I. Rovira,¹ Daniel Schimel,⁵ Calvin J. Kuo,⁶ J. Silvio Gutkind,² Paul M. Hwang,¹ Toreen Finkel^{1†}

The contribution of stem and progenitor cell dysfunction and depletion in normal aging remains incompletely understood. We explored this concept in the *Klotho* mouse model of accelerated aging. Analysis of various tissues and organs from young *Klotho* mice revealed a decrease in stem cell number and an increase in progenitor cell senescence. Because *klotho* is a secreted protein, we postulated that *klotho* might interact with other soluble mediators of stem cells. We found that *klotho* bound to various Wnt family members. In a cell culture model, the Wnt-*klotho* interaction resulted in the suppression of Wnt biological activity. Tissues and organs from *klotho*-deficient animals showed evidence of increased Wnt signaling, and ectopic expression of *klotho* antagonized the activity of endogenous and exogenous Wnt. Both in vitro and in vivo, continuous Wnt exposure triggered accelerated cellular senescence. Thus, *klotho* appears to be a secreted Wnt antagonist and Wnt proteins have an unexpected role in mammalian aging.

Resident and circulating stem and progenitor cells are critical for ongoing tissue maintenance and repair, and it is often postulated that stem and progenitor cell depletion or dysfunction might contribute to aging (1). We therefore examined stem cell dynamics in a genetic model of accelerated aging. Mice lacking *klotho* expression, henceforth termed *Klotho* mice, have a shortened life span and exhibit a number of early-onset age-related changes, including arteriosclerosis, decreased fertility, and skin atrophy (2). *Klotho* is a transmembrane protein with a large extracellular domain composed of two repeats (KL1 and KL2 domains) that share similarity to Family I glycosidases. In addition to being cell-associated, the extracellular portion of

klotho is secreted and can be detected in the circulation of animals and humans (3). It is generally believed that secreted *klotho* is the form most likely mediating the protein's longevity effects.

One alteration in *Klotho* animals is the early appearance of age-related changes in the skin. To assess whether these phenotypic changes were accompanied by alterations in stem cell number, we identified the number of long-term 5-bromo-2'-deoxyuridine (BrdU)-retaining cells in the skin of either wild-type or age-matched *Klotho* animals (4). These label-retaining cells (LRCs) are a convenient method to identify stem cells within their niche (5). At an age of 2.5 months, *Klotho* mice had significantly fewer LRCs than their wild-type littermates [wild type: 80 ± 5 LRCs (\pm SD) per set of three follicles versus *Klotho*: 35 ± 3 LRCs, $n = 30$, $P < 0.05$ paired t test]. Skin LRCs are confined to a specialized region of the follicle known as the bulge region, and the stem cells contained within this niche are enriched for CD34 expression (6). The bulge region in *Klotho* animals was consistently smaller with reduced CD34 expression (Fig. 1A). Hair follicle epidermal stem cells are also a source of transient amplifying (TA) cells induced by acute wounding (7). Consistent with a defect in the number of LRCs, epidermal wounding resulted in a diminished number of TA cells in

the *Klotho* animals (Fig. 1B) and a deficit in wound closure (Fig. 1C).

Age-matched wild-type and *Klotho* skin sections also exhibited differences in senescence-associated endogenous β -galactosidase (SA β -gal) activity (Fig. 1D). The observed SA β -gal staining occurred in the outermost epidermal layer including the acellular stratum corneum. The specificity and physiological significance of this staining is unclear. Examination of numerous random follicles revealed that the *Klotho* animals also had intense β -galactosidase staining within the follicles, especially within regions known to contain rapidly dividing progenitor cells (8). We observed little to no SA β -gal staining in the intra-follicular regions. Senescent cells often activate the DNA damage response (DDR) pathway, as evidenced by the development of nuclear foci of proteins such as phosphorylated histone (H2AX), ataxia telangiectasia mutated (ATM), and binding protein 1 (53BP1) (9). The DDR pathway was activated in multiple random *Klotho* follicles but not in age-matched wild-type mice (Fig. 1D).

Klotho animals also demonstrated increased SA β -gal staining in the small intestine, especially within intestinal crypts, an area enriched for stem and progenitor cells (Fig. 1E). Similar analysis of the testis in male animals also demonstrated evidence of increased progenitor cell senescence (fig. S1). In the bone marrow of *Klotho* mice, there was also a reduction in the population of cells bearing the cell surface phenotype of c-kit⁺ sca-1⁺ lineage negative that encompasses the hematopoietic stem cell (HSC) (Fig. 1F). This reduction of HSC in *Klotho* animals was accompanied by a marked increase in the percentage of stem cells that were actively dividing (*Klotho* HSCs: $28.4 \pm 3.7\%$ in G₁ versus wild-type HSCs: $10.2 \pm 1.1\%$ in G₁, $n = 3$ animal pairs per group, $P < 0.05$ paired t test) (Fig. 1G).

Given that stem cell biology is regulated by a number of secreted factors, we wondered whether there might be a functional interaction between *klotho* and one of these known stem cell regulators. In the course of our experiments, we noted that the subcellular distribution of *klotho* and Wnt proteins within transfected cells overlapped (fig. S2). Thus, we sought to determine whether *klotho* and Wnt3 could form a direct molecular complex. Epitope-tagged Wnt3 and myc-tagged *klotho* were readily detectable in transfected cell lysates (Fig. 2A). *Klotho* associated with immu-

¹Cardiology Branch, National Heart, Lung, and Blood Institute, NIH, Bethesda, MD 20892, USA. ²Oral and Pharyngeal Cancer Branch, National Institute of Dental and Craniofacial Research, NIH, Bethesda, MD 20892, USA. ³Hematology Branch, National Heart, Lung, and Blood Institute, NIH, Bethesda, MD 20892, USA. ⁴Light Microscopy Core Facility, National Heart, Lung, and Blood Institute, NIH, Bethesda, MD 20892, USA. ⁵Mouse Imaging Facility, NIH, Bethesda, MD 20892, USA. ⁶Division of Hematology, Stanford University School of Medicine, Stanford, CA 94305, USA.

*These authors contributed equally to this work.

†To whom correspondence should be addressed. E-mail: finkel@nih.gov

nonprecipitated Wnt3, and the reciprocal immunoprecipitation of *klotho* contained Wnt3 (Fig. 2A). A single extracellular KL domain was sufficient to mediate the observed interaction with Wnt3 (Fig. 2B). The Wnt binding domain was contained within the amino-terminal portion of *klotho*'s KL1 domain (amino acids 1 to 285) (fig. S3). Full-length *klotho* also immunoprecipitated with a number of other Wnt isoforms including Wnt1, Wnt4, and Wnt5a (fig. S4).

We further analyzed the biological effects of the observed *klotho*/Wnt interaction. We coexpressed Wnt3 and *klotho* in human embryonic kidney (HEK) 293 cells along with a Wnt-responsive reporter. The presence of Wnt3 increased reporter activity by approximately 7 times, whereas the addition of increasing amounts of *klotho* reduced Wnt activity in a dose-dependent fashion (Fig. 2C). Various structural mutants containing a single KL1 domain or altering conserved amino acids believed to be important in *klotho*'s β -glucuronidase activity failed to abrogate *klotho*-mediated Wnt inhibition (fig. S5). In contrast, *klotho* constructs that failed to physically interact with Wnt3 also failed to inhibit Wnt activity (fig. S6).

We next asked whether *klotho* could inhibit Wnt activity in a cell-free system. Conditioned media with and without either *klotho* or Wnt3a were prepared and mixed in various combinations before being placed on HEK-293 cells transfected with a Wnt reporter construct. These results indicated that secreted *klotho* could inhibit soluble Wnt activity (Fig. 2D). In contrast, secreted *klotho*-conditioned medium was ineffective in inhibiting Wnt signaling directly stimulated by intracellular β -catenin expression (fig. S7).

We next tested whether animals lacking *klotho* expression had increased Wnt activity. We crossed *Klotho* animals with the TOPGAL reporter strain in which the activity of a β -galactosidase reporter is under the control of Wnt-responsive elements (10). Analysis of the skin of *Klotho*/TOPGAL animals demonstrated an increase in β -galactosidase reporter activity compared with that of age-matched wild-type/TOPGAL controls (Fig. 3A). Quantitative analysis confirmed this augmented Wnt activity in the skin and small intestine of *Klotho* mice and demonstrated that the increased expression of the Wnt-dependent β -galactosidase reporter was similar to that of *Axin2*, a known Wnt target gene (fig. S8). Other potential transcriptional targets of the Wnt pathway also showed increased transcription in *Klotho* animals (fig. S9).

Whereas normal aging is associated with bone loss, studies in mice and humans have established that augmented Wnt signaling leads to increased bone mass (11). We therefore monitored Wnt activity in bones of aged-matched wild-type or *Klotho* littermates. Using the TOPGAL reporter, we detected augmented reporter activity in sections obtained from the proximal tibia of 2-week-old *Klotho* mice (Fig. 3B and fig. S10). At this time point, *Klotho* mice lack any

discernible phenotype, suggesting that the increase in Wnt activity precedes the apparent onset of accelerated aging. We also analyzed by microcomputerized tomography (μ CT) the tibias of 3-month-old wild-type or *Klotho* animals. *Klotho* mice demonstrated nearly 5 times as much tibial trabecular bone mass (Fig. 3, C to E). An increase in overall tibial and vertebral column trabecular bone density has actually been previously noted but unexplained in *Klotho* mice (12).

In contrast, other bones in the *Klotho* animals exhibit decreased bone density (2). The basis for this regional difference in bone density is unclear but may relate to the complex interplay of *klotho*'s ability both to alter Wnt signaling and to regulate other pathways involved in calcium and vitamin D homeostasis (13–16).

To test whether augmented *klotho* expression could inhibit Wnt signaling in vivo, we analyzed TOPGAL reporter mice in the first few weeks of

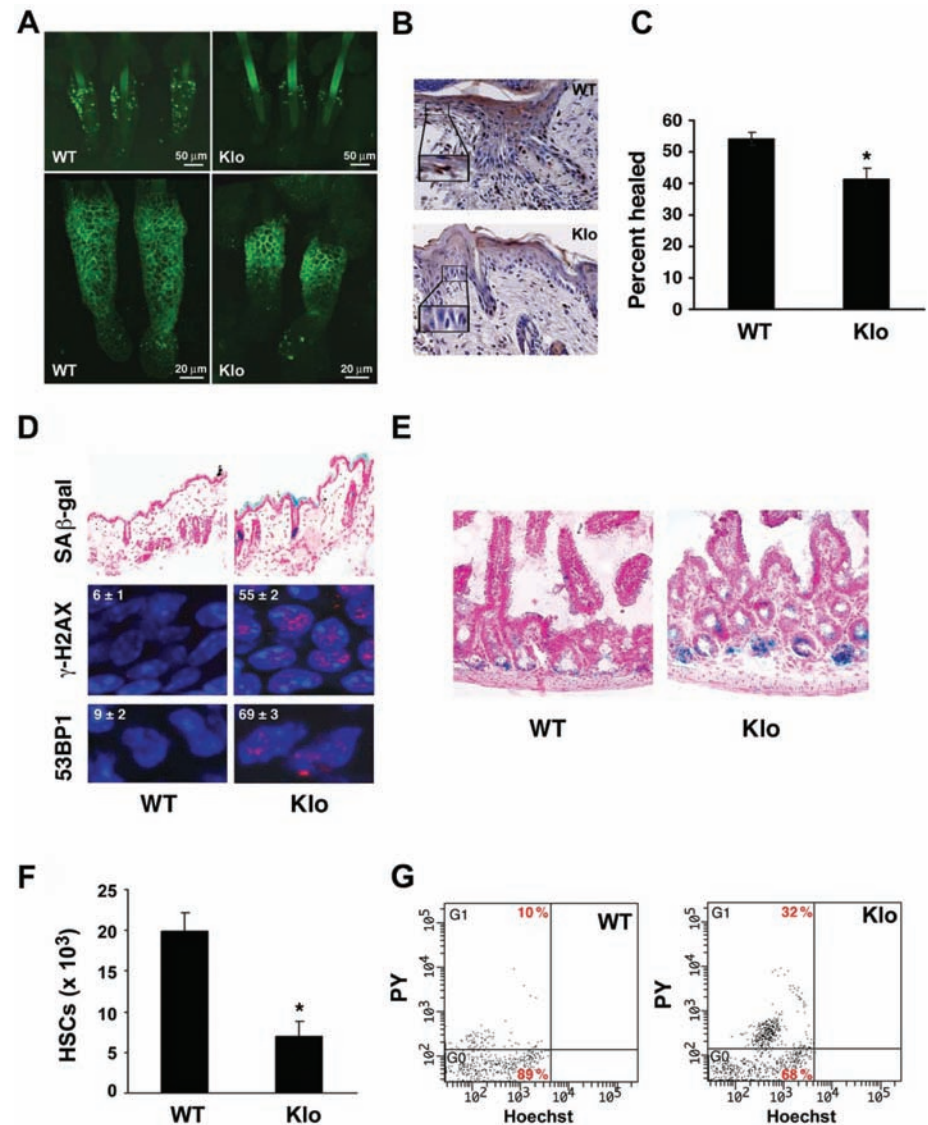


Fig. 1. Altered stem and progenitor cells in *Klotho* mice. (A) LRCs within the skin follicles of 80-day-old wild-type (WT) or *Klotho* (Klo) mice (top). Higher magnification of representative bulge regions stained for CD34 (bottom). (B) TA cells, identified by positive brown nuclear BrdU staining, after skin wounding. (C) Assessment of skin closure 4 days after creating a 1-cm wound ($n = 4$ pairs, $*P < 0.05$ paired t test). (D) Evidence for senescence within the hair follicle of *Klotho* animals as assessed by β -gal staining (SA β -gal) and nuclear foci of γ -H2AX and 53BP1 (red) in 4',6'-diamidino-2-phenylindole (DAPI)-stained nuclei (blue). Percentage of positive nuclear staining in either wild-type or *Klotho* follicles is shown \pm SD. (E) SA β -gal staining of small intestine. (F) Determination of the absolute number of c-kit⁺sca-1⁺ Lin⁻ HSCs in bilateral femur and tibiae of either wild-type or *Klotho* animals ($n = 3$ pairs, $*P < 0.05$ paired t test). (G) Representative cell cycle analysis of HSCs from wild-type and *Klotho* animals demonstrating a decrease in HSC quiescence (% G₀) and increased proliferation (% G₁). DNA content is displayed along the x axis; RNA content determined by Pyronin Y (PY) staining is displayed along the y axis.

life, when the kinetics of the hair follicle cycle are synchronized (17). On postnatal day 8, mice were injected subcutaneously with one of three dif-

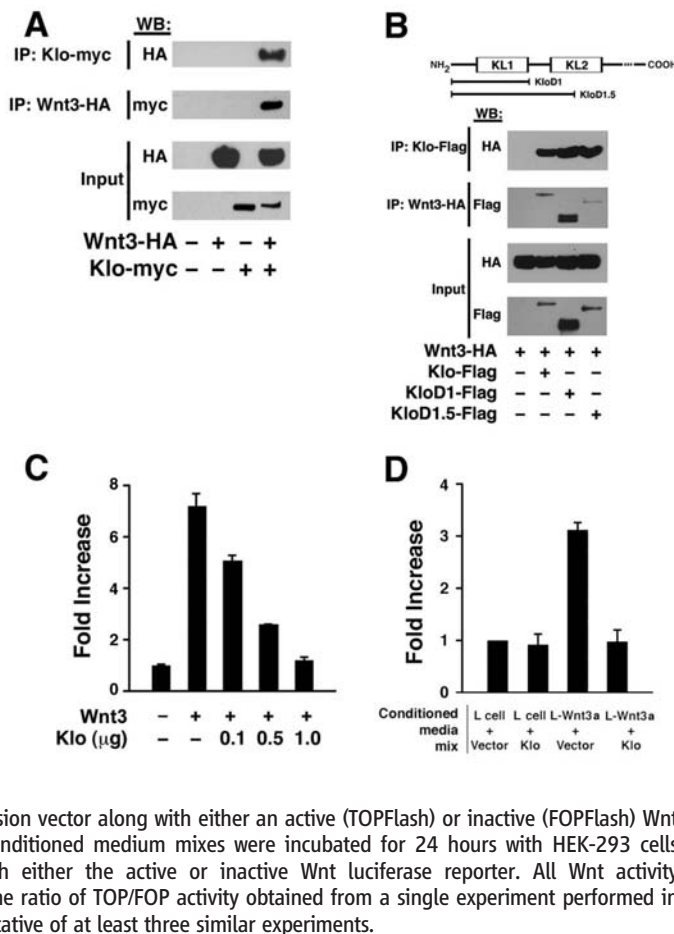
ferent recombinant adenoviruses encoding either klotho (Ad.Klo), the Wnt inhibitor DKK-1 (Ad.DKK1), or an adenovirus encoding the

immunoglobulin G Fc fragment (Ad.Fc) that served as a control. Four days after injection (postnatal day 12), we harvested the injected area and assessed Wnt activity in the hair follicle. In control-injected skin, Wnt activity was clearly visible around numerous growing hair follicles, whereas this activity was reduced in both the DKK-1 and klotho injected skin (fig. S11). Assessment of more than 500 random follicles in each condition revealed that klotho was roughly equivalent to DKK-1 in the ability to quantitatively suppress Wnt's biological activity (Fig. 3F).

To assess whether the expression of klotho could also block the effects of pathological Wnt expression, we crossed two strains of mice, one that expressed the tetracycline-inducible transcriptional activator (rtTA) under the control of the cytokeratin 5 promoter (K5rtTA) and another that expressed Wnt1 under the control of multiple *tet*-responsive elements (*tet*-Wnt1) (18, 19). The resultant cross generated the experimental line K5rtTA/*tet*-Wnt1, which provided tetracycline-inducible expression of Wnt1 in the basal layer of stratified epithelium. In our transgenic animals, ectopic expression of Wnt1 from postnatal day 12 to 21 resulted in increased epidermal thickness and marked follicular hyperplasia (Fig. 3G). The local injection of either DKK-1 or klotho, but not the control adenovirus, blocked these pathological Wnt-induced skin changes (Fig. 3G).

To begin to directly assess the role of Wnt proteins in aging, we tested whether continuous Wnt exposure induced cellular senescence. We grew primary mouse embryonic fibroblasts (MEFs) in the presence or absence of Wnt3a-conditioned medium. Consistent with Wnt proteins having mitogenic effects, analysis of BrdU

Fig. 2. Interaction of klotho with Wnt and inhibition of Wnt signaling. (A) HEK-293 cells were transiently transfected with myc- and hemagglutinin (HA)-tagged expression constructs encoding Wnt3 and murine klotho (Klo). Reciprocal coimmunoprecipitation (IP) of klotho and Wnt3 from cell lysates is also demonstrated. WB, Western blot. (B) Schematic diagram of klotho demonstrating the two extracellular klotho repeats (KL1 and KL2) followed by the single-pass transmembrane domain (-). Flag-tagged full-length klotho (Klo) and truncation mutants were assessed for Wnt binding. (C) HEK-293 cells were transfected with a Wnt3 expression construct (100 ng DNA) and the indicated amount of



a full-length klotho expression vector along with either an active (TOPFlash) or inactive (FOPFlash) Wnt luciferase reporter. (D) Conditioned medium mixes were incubated for 24 hours with HEK-293 cells previously transfected with either the active or inactive Wnt luciferase reporter. All Wnt activity measurements represent the ratio of TOP/FOP activity obtained from a single experiment performed in triplicate and are representative of at least three similar experiments.

Fig. 3. Inhibition of Wnt signaling by klotho in vivo. (A) Endogenous Wnt activity in skin from 14-day-old wild-type or Klotho mice crossed with the TOPGAL reporter strain. (B) Wnt activity in tibias of 14-day-old Klotho/TOPGAL or wild-type/TOPGAL mice. (C) Longitudinal microcomputerized CT sections from the tibia of 3-month-old Klotho (top) or wild-type (bottom) animals. (D) Horizontal three-dimensional reconstruction of cortical bone (yellow) and trabecular bone (green). (E) Calculation of the trabecular to total bone volume from the tibia of three pairs of 3-month-old wild-type or Klotho animals. (F) Quantification of the percentage of β-galactosidase positive follicles from 12-day-old TOPGAL mice injected 4 days earlier with either a control virus (Ad.Fc), an adenovirus encoding the Wnt inhibitor (Ad.DKK1), or an adenovirus encoding klotho (Ad.Klo). Approximately 500 random follicles were assessed per condition. (G) Hyperplastic skin phenotype of K5rtTA/*tet*-Wnt1 transgenic mice treated with doxycycline is blocked by prior injection of an adenovirus encoding for either DKK-1 or klotho. Mice were killed on postnatal day 21.

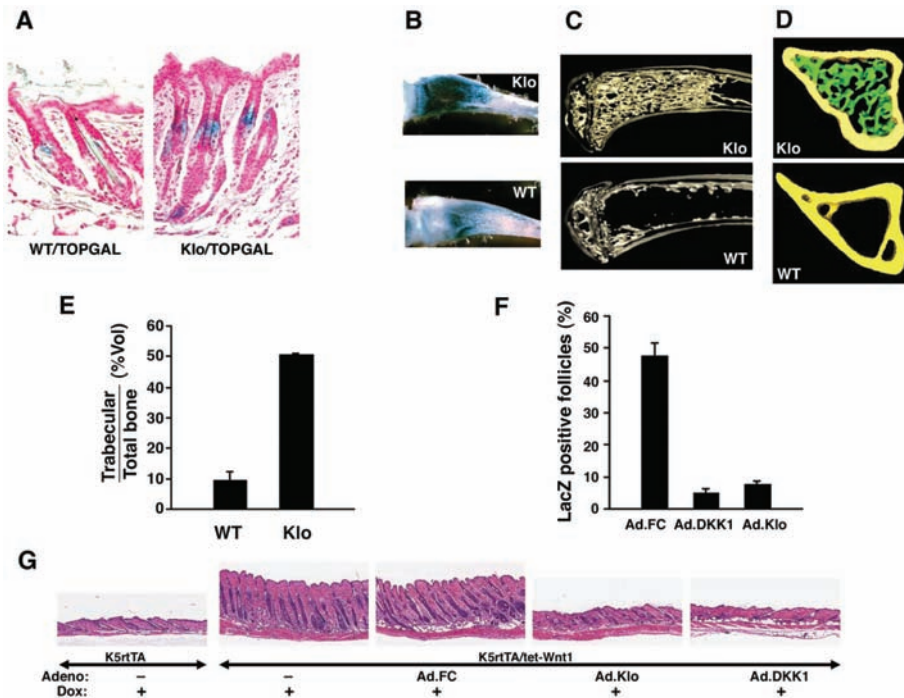
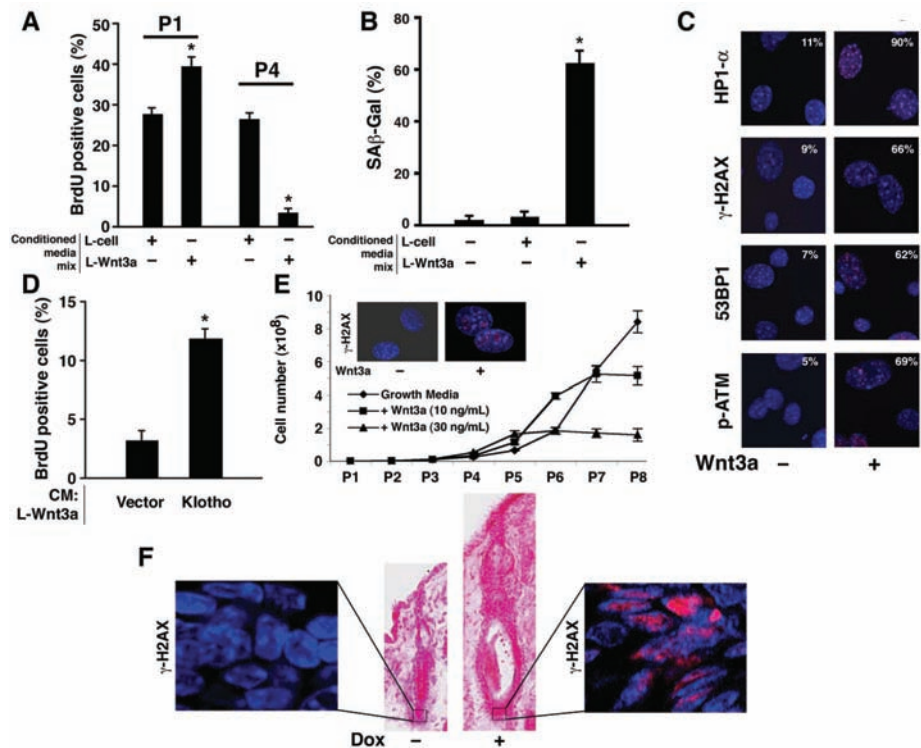


Fig. 4. Senescence induced by increased Wnt activity. **(A)** BrdU incorporation for MEFs grown in the presence or absence of Wnt3a conditioned media. Cells were assayed from passage 1 (P1) through passage 4 (P4). **(B)** Senescence associated β -galactosidase staining (SA β -gal) for MEFs (P4) grown in standard media (–) or mixed with the indicated L-cell conditioned medium. **(C)** MEFs (P4) with or without continuous Wnt3a exposure were assessed for senescence-associated heterochromatin (HP1- α) and the activation of the DNA damage response. **(D)** Level of BrdU incorporation (P4) for MEF cells continuously treated with L-Wnt3a conditioned media (CM) mixed with either vector-transfected or klotho-transfected conditioned medium. **(E)** Growth of MEFs in standard medium (diamonds), or supplemented with Wnt3a at 10 ng/ml (squares) or 30 ng/ml (triangles). (Inset) P7 cells were stained for activation of H2AX. **(F)** Skin sections obtained from K5rtTA/*tet*-Wnt1 transgenic mice either treated or untreated with doxycycline (Dox) from postnatal days 2 through 21. The senescence-associated marker γ -H2AX is induced in the setting of continuous in vivo Wnt1 (+Dox) exposure.



incorporation revealed that Wnt-conditioned medium initially acted to increase MEF cell proliferation (Fig. 4A). However, over time, continuous Wnt exposure resulted in a marked decrease in proliferation (Fig. 4A and fig. S12). Wnt exposure did not increase the level of apoptosis (fig. S13); rather, assessment of cells grown in the continuous presence of Wnt3a demonstrated a flattened morphology with evidence of increased SA β -gal activity (Fig. 4B and fig. S14). Similarly, continuous Wnt3a exposure triggered the DDR pathway as well as nuclear foci of HP1- α , a marker of senescence-associated heterochromatin formation (Fig. 4C). The inhibitory effects of long-term Wnt3a-conditioned media on MEF proliferation (fig. S15) and BrdU incorporation (Fig. 4D) were attenuated by the addition of soluble klotho. Similar results were obtained with purified Wnt3a protein rather than Wnt3a-conditioned medium (Fig. 4E and fig. S16) and when using human rather than mouse cells (fig. S17).

Finally, we tested whether Wnt could induce senescence in vivo by analyzing the skin of K5rtTA/*tet*-Wnt1 transgenic animals. Beginning on postnatal day 2, littermate transgenic animals were placed on a diet with or without doxycycline (Dox) and skin samples were collected for study on day 21. Analysis of multiple random follicles ($n > 100$) demonstrated an increase in senescence markers in those animals exposed to continuous Wnt1 expression. On day 21, 70% of the follicles in Wnt1-expressing animals exhibited staining for γ -H2AX, whereas less than 5% of uninduced follicles demonstrated this phenotype (Fig. 4F). Similarly, whereas follicles from

young animals without Dox treatment showed little to no evidence of senescence, their Wnt1-induced littermates demonstrated multiple areas of discrete SA β -gal staining (fig. S18).

We demonstrate that klotho acts as a Wnt antagonist and that chronic Wnt stimulation may contribute to stem cell depletion and aging. During the course of our studies, two other studies appeared demonstrating that forced constitutive Wnt signaling within HSC led to a rapid exhaustion of long-term repopulating stem cells (20, 21). These results, as well as the observations in Brack *et al.* (22), are broadly consistent with our observations of Klotho mice. Previous attempts to understand the basis of the observed Klotho aging phenotype have implicated alterations in insulin signaling as well as, more recently, the fibroblast growth factor 23 pathway (14–16, 23). Further analysis is therefore required to fully understand how these various klotho-regulated pathways potentially intersect and whether any biological hierarchy exists. Nonetheless, our results provide an unexpected connection between aging and the well-studied Wnt signaling pathway and suggest that strategies targeting soluble mediators of stem cell function may provide new therapeutic strategies to combat aging and potentially age-related diseases.

References and Notes

1. T. A. Rando, *Nature* **441**, 1080 (2006).
2. M. Kuro-o *et al.*, *Nature* **390**, 45 (1997).
3. N. M. Xiao, Y. M. Zhang, Q. Zheng, J. Gu, *Chin. Med. J. (Engl.)* **117**, 742 (2004).
4. Materials and methods are available as supporting material on Science Online.
5. K. M. Braun, F. M. Watt, *J. Invest. Dermatol. Symp. Proc.* **9**, 196 (2004).

6. T. Tumber *et al.*, *Science* **303**, 359 (2004).
7. M. Ito *et al.*, *Nat. Med.* **11**, 1351 (2005).
8. C. Blanpain, E. Fuchs, *Annu. Rev. Cell Dev. Biol.* **22**, 339 (2006).
9. D. B. Lombard *et al.*, *Cell* **120**, 497 (2005).
10. R. DasGupta, E. Fuchs, *Development* **126**, 4557 (1999).
11. V. Krishnan, H. U. Bryant, O. A. Macdougald, *J. Clin. Invest.* **116**, 1202 (2006).
12. T. Yamashita, Y. Nabeshima, M. Noda, *J. Endocrinol.* **164**, 239 (2000).
13. Q. Chang *et al.*, *Science* **310**, 490 (2005).
14. H. Kurosu *et al.*, *J. Biol. Chem.* **281**, 6120 (2006).
15. M. S. Razaque, D. Sitara, T. Taguchi, R. St-Arnaud, B. Lanske, *FASEB J.* **20**, 720 (2006).
16. I. Urakawa *et al.*, *Nature* **444**, 770 (2006).
17. E. Fuchs, *Nature* **445**, 834 (2007).
18. L. Vitale-Cross, P. Amornphimoltham, G. Fisher, A. A. Molinolo, J. S. Gutkind, *Cancer Res.* **64**, 8804 (2004).
19. E. J. Gunther *et al.*, *Genes Dev.* **17**, 488 (2003).
20. M. Scheller *et al.*, *Nat. Immunol.* **7**, 1037 (2006).
21. P. Kirstetter, K. Anderson, B. T. Porse, S. E. Jacobsen, C. Nerlov, *Nat. Immunol.* **7**, 1048 (2006).
22. A. S. Brack *et al.*, *Science* **317**, 807 (2007).
23. H. Kurosu *et al.*, *Science* **309**, 1829 (2005).
24. We thank R. Moon for the Wnt (TOP/FOP) reporter constructs, M. Kuro-o for generating the *klotho* mice, and H. Dietz for providing the *klotho* mice. The TOPGAL mouse was generated by E. Fuchs and kindly provided by Y. Yang. We also thank J. G. Kang for technical help. This work was supported by Intramural NIH funds (T.F.), a grant from the Ellison Medical Foundation (T.F.), and an NIH 1 R01 DK069989-01 to C.J.K.

Supporting Online Material

www.sciencemag.org/cgi/content/full/317/5839/803/DC1
 Materials and Methods
 Figs. S1 to S18
 References

9 April 2007; accepted 9 July 2007
 10.1126/science.1143578